ENVIRONMENTAL RESEARCH
LETTERS

PURPOSE-LED PUBLISHING™ Part of the ENVIRONMENTAL RESEARCH SERIES

LETTER • OPEN ACCESS

Winter sea surface temperature interhemispheric dipole as a predictor for Sahel summer rainfall

To cite this article: Ahmad Abdullahi Bello and Jianping Li 2025 *Environ. Res. Lett.* **20** 104033

ENVIRONMENTAL RESEARCH
LETTERS

LETTER

Winter sea surface temperature interhemispheric dipole as a predictor for Sahel summer rainfall

Ahmad Abdullahi Bello[1,3] **and Jianping Li**[1,2,*]

[1] Frontiers Science Center for Deep Ocean Multispheres and Earth System (DOMES)/ Key Laboratory of Physical Oceanography/Academy of Future Ocean/College of Oceanic and Atmospheric Sciences/Center for Ocean Carbon Neutrality, Ocean University of China, Qingdao 266100, People's Republic of China
[2] Laboratory for Ocean Dynamics and Climate, Qingdao Marine Science and Technology Center, Qingdao 266237, People's Republic of China
[3] National Weather Forecasting and Climate Research Center, Nigerian Meteorological Agency (NiMet), Abuja, Nigeria
[*] Author to whom any correspondence should be addressed.

E-mail: ljp@ouc.edu.cn

Keywords: West African monsoon (WAM), climate prediction, intertropical convergence zone (ITCZ), air-sea interaction

Supplementary material for this article is available online

OPEN ACCESS

RECEIVED
15 June 2025

REVISED
26 August 2025

ACCEPTED FOR PUBLICATION
2 September 2025

PUBLISHED
9 September 2025

Abstract

Skillful prediction of Sahel summer rainfall (SSR) is critical for mitigating hydrometeorological disasters in this vulnerable climate hotspot. In this study, we employ observational analysis from 1950–2023 to show that the sea surface temperature interhemispheric dipole in winter (SSTIDw) has a strong influence on SSR. A positive SSTIDw anomaly-marked by relatively warmer Northern Hemisphere sea surface temperatures-persists through spring to summer and leads to persistent negative surface pressure anomalies and anomalous cyclonic circulation. This intensifies the Saharan heat low and reinforces anomalous westerly and southwesterly flows across the Atlantic and the Guinea Coast, enhancing moisture flux convergence and rainfall in the Sahel. Based on this relationship, we develop an SSTIDw-based linear regression model that skillfully captures SSR characteristics. These findings highlight the multi-month lead time predictability of SSR, which is critical for climate-informed decision making in the Sahel.

1. Introduction

The West African Monsoon (WAM) accounts for a significant part of the Sahel summer rainfall (SSR) observed during the rainy season (July–September) (Thorncroft *et al* 2011, Biasutti 2019). Throughout this period of heightened hydrological activity, agricultural activities flourish to serve as a major source of sustenance for local communities. At an interannual time scale, surface pressure contrast between the Sahara and the tropical Atlantic Ocean interacts to shape the atmospheric dynamics that control rainfall variability in the Sahel (Nicholson and Webster 2007). However, the pronounced sensitivity of the Sahel to this variability over short or extended periods implies that even small fluctuations in circulation patterns could result in significant regional impacts (Nicholson 2018), highlighting the need for skillful prediction.

Extensive research has highlighted the essential role of sea surface temperature (SST) in forcing Sahel rainfall variability at different time scales (Folland *et al* 1986, Giannini *et al* 2003, Mohino *et al* 2011, Pomposi *et al* 2016, Diakhaté *et al* 2019). However, the forcing of distinct SST basins on Sahel rainfall is non-stationary (Losada *et al* 2012, Suárez Moreno 2019). For instance, while a marked disassociation between Sahel rainfall and tropical North Atlantic occurred after the 1970s, the El Niño-Southern Oscillation teleconnection signal began to strengthen at a comparable time (Janicot *et al* 2001, Losada *et al* 2012). Globally, the interhemispheric SST gradient influences rainfall in tropical land regions (Folland *et al* 1986, Sun *et al* 2013). Defined as the northern hemisphere minus the southern hemisphere (NH-SH) SST (Sun *et al* 2013, An *et al* 2024), the SST interhemispheric dipole (SSTID) is a global mode of SST variability that triggers global-scale change in

atmospheric circulation with direct influence on HN summer monsoon (Xue *et al* 2022).

Accuracy and lead time are arguably the two most important factors determining any prediction system's value. Despite the commendable progress made in the skillful prediction of the SSR using both statistical and dynamical methods, there remains an avenue for improvement (Folland *et al* 1991, Badr *et al* 2014, Sheen *et al* 2017, Giannini *et al* 2020, Martín-Gómez *et al* 2022). In dynamical models, poor skill is primarily attributed to inadequate representation of SSTs and their teleconnections with the SSR. Notably, poor representation of the dominant sources of skill, such as the global tropical Oceans, the North Atlantic Ocean, and the Mediterranean Sea, leads to amplified biases in dynamical models (Giannini *et al* 2020, Martín-Gómez *et al* 2022). On the other hand, statistical models leverage on identifying high-skill predictors at relevant lead times. Consequently, studies have found preceding large-scale SSTs and other variables form the basis for skillful SSR prediction (Badr *et al* 2014, Folland *et al* 1991, Mo and Thiaw 2002, Yaqian and Lee 2016). However, preceding large-scale SST signals exert more influence on SSR that is more robust and stationary compared to indices derived from individual oceanic basins (Folland *et al* 1991). For instance, Folland *et al* (1991) demonstrated the dominance of global SST over regional SST modes during the preceding spring in explaining SSR variability. Similarly, Badr *et al* (2014) maintained the same lead time (spring) to highlight the value of SST and surface air temperature in predicting SSR, with the best skill produced by employing artificial neural network (ANN), stemming from its ability to capture nonlinear relationships with large-scale variables.

In this study, we maintain the dominance of the global-scale SST mode (SSTID) and demonstrate that a significant association between this mode and SSR not only exists in the preceding winter but is also the strongest, and the possible mechanism for this time-lag relationship is explored. Moreover, we leverage this relationship to build a predictive model, as a reliable forecast issued at sufficient lead time increases forecast value through early action initiation, particularly in vulnerable communities where social and human factors impede the timely delivery of forecast products (Hulme *et al* 1992, Islam *et al* 2025).

2. Data and methods

2.1. Data

This study uses monthly Climate Research Unit Time Series Version 4.08. This is high-resolution (0.5° latitude × 0.5° longitude) observation-based rainfall data that covers the year 1901 to the present and employs the angular-distance weighting method for interpolation (Harris *et al* 2020). We also use monthly SST data from extended reconstructed SST Version 5, which is global with a horizontal resolution of 2° × 2°, available from 1854 to the present and suitable for long-term analysis (Huang *et al* 2017). Monthly horizontal wind, specific humidity, vertical velocity, outgoing long wave radiation, and sea level pressure (SLP) data were obtained from the National Centers for Environmental Prediction/National Center for Atmospheric Research Reanalysis 1. This atmospheric model output is available globally and monthly from 1948 to the present at 2.5° × 2.5° resolution (Kalnay *et al* 1996). A uniform period of 1950–2023 was used in all datasets.

2.2. Methods

First, we calculated the monthly SSTID index as the SST difference between the NH and SH SST following Sun *et al* (2013) and An *et al* (2024). Then, seasonal averages are computed for D(−1)JF, JFM, …, JAS seasons, where D(−1) is the previous year's December. Hence, SST interhemispheric dipole in winter (SSTIDw) and SSTIDs represent winter [D(−1)JF] and summer (JAS) SSTID, respectively. We define the SSR index as July–September (JAS) standardized area-averaged rainfall over 10°N–20°N and 20°W–40°E as in (Giannini *et al* 2003, Yujun He *et al* 2024). Correlation and regression analysis were used to study the relationship between variables, and the Student's *t*-test was applied to test significance. Furthermore, we analyzed consistent temporal coverage (1950–2023) in all variables. An empirical model was trained using simple linear regression, where SSR (SSTIDw) is the response (predictor) variable. 1950–2001 was designated the training period, while 2002–2023 was used for independent validation. Evaluation metrics, including correlation coefficient (r), root mean square error (RMSE), and sign consistency (SC), were used to assess model performance. Linear trends were removed from all variables to reduce the effect of global warming.

3. Results

3.1. SSTID and SSR relationship

We examine the correlation of SSR with seasonal SSTID indices in the concurrent and prior seasons. The evolution of the correlation coefficients indicates that the SSR and SSTID are significantly and persistently correlated. While significant positive correlations exceeding 0.5 ($p < 0.05$) persist from winter to summer, the strongest is found between SSR and the SSTIDw (figure 1(a)). The time series of SSR and SSTIDw further demonstrates the strength of this relationship, with a significant correlation coefficient of 0.65 (figure 1(b)). Folland *et al* (1991) found broadly consistent results, although with slightly different definitions of the interhemispheric dipole (making the northern Indian Ocean part of the SH ocean and dividing the two hemispheres at 5° N).

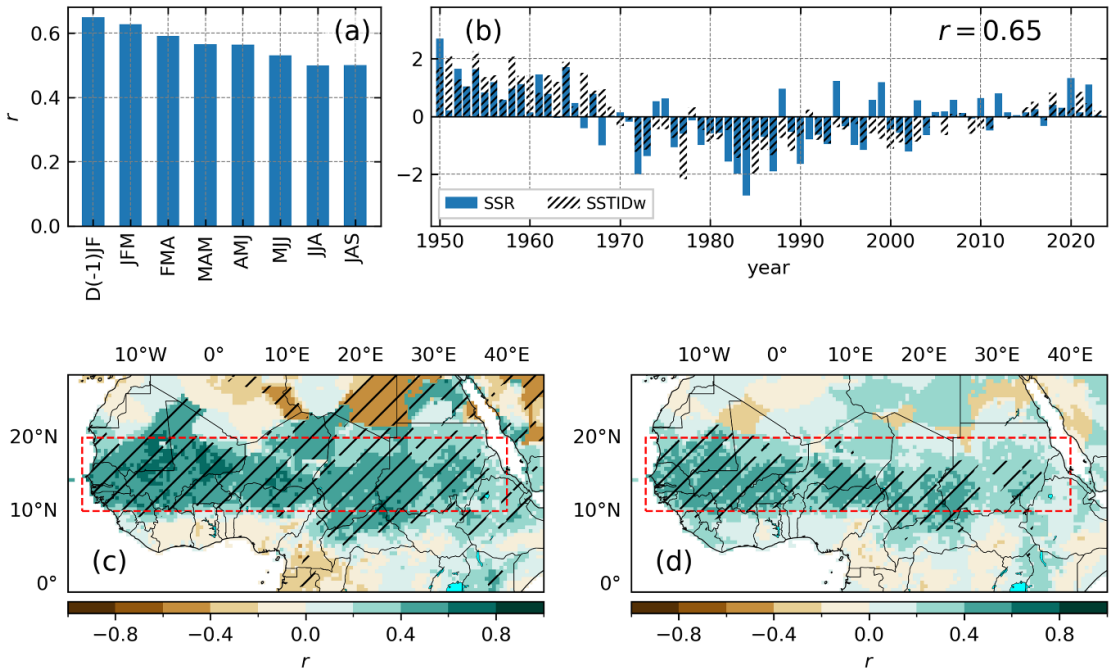

Figure 1. (a) Lead-lag correlation coefficients between the SSR index and seasonal SSTID indices, spanning D(−1)JF to JAS. (b) Standardized time series of the SSR index (blue bars) and SSTIDw (black bars). (c) Correlation map of SSTIDw with JAS rainfall over tropical northern Africa; shading indicates significance at the 5% level. (d) As in (c) but for SSTIDs. The red dashed box in (c) and (d) denotes the Sahel region used for SSR calculation. Period: 1950–2023; shadings indicate significance at 5% level; anomalies in (b) are relative to 1981–2010 climatology.

Additionally, the SSR and SSTIDw time series are characterized by strong interannual to decadal variability. Particularly, the magnitude of the wet periods of the 1950s–60s and the dry periods of the 1970s–80s is strongly harmonized with the SSTIDw. In contrast, the recent period exhibits relatively less magnitude of undulating wet and dry periods. The SSR time series typically resembles Sahel rainfall presented in previous studies, with varying observations and slightly different areas considered (Biasutti 2013, Nicholson *et al* 2018). Correlation maps of SSR with the prior SSTIDw (figure 1(c)) and simultaneous SSTIDs (figure 1(d)) are further examined. The correlation map between SSR and SSTIDs indicates robust and statistically significant ($r > 0.65$, $p < 0.01$) correlations across the entire Sahel region (figure 1(c)). However, the correlations with SSTIDs are relatively weaker and less spatially consistent, particularly in parts of the northeastern Sahel (figure 1(d)).

SST variations in key ocean regions, such as the global tropical oceans, the North Atlantic, and the Mediterranean Sea exert significant influence on SSR (Giannini *et al* 2003, Sheen *et al* 2017). During this season, we found that the SSTIDs–SSR relationship is robust and stationary, comparable to that of the Mediterranean Sea (figure S1(a)). Moreover, SSTIDw maintains a robust and statistically significant relationship with SSR, not evident in other regional SST signals (figure S1(b)).

3.2. Circulation features and physical mechanism

To assess how the SSTIDw modulates the circulation anomalies over the Sahel, we compute regression anomalies of SLP and 850 hPa winds against the SSTIDw index, focusing on the seasonal evolution from winter to summer (figure 2). During the positive phase of SSTIDw, we observe a notable change in sub-tropical pressure systems. In the SH, anomalous low pressure dominates, strengthening and becoming more pronounced in summer (figure 2(c)). On the other hand, an anomalous cyclonic circulation emerges in the North Atlantic at approximately 50°N during spring. This system subsequently propagates eastward and weakens slightly by summer. Simultaneously, a seasonally persistent low-pressure anomaly emerges over the Sahara, with the maximum amplitude shifting westward across the Sahara. This signals a robust strengthening of the Saharan heat low (SHL). The associated cyclonic circulation within the SHL reinforces anomalous westerly and southwesterly flows to its south, thereby strengthening the WAM (Parker *et al* 2005, Raj *et al* 2019). Both observational and modeling studies have highlighted the relationship between the SHL and the SSR(Haarsma *et al* 2005, Shekhar and Boos 2017). As demonstrated by Shekhar and Boos (2017), SHL intensification associated with low-level geopotential height reduction induces a northward shift of Saharan shallow meridional circulation (SMC) and wetting of the Sahel.

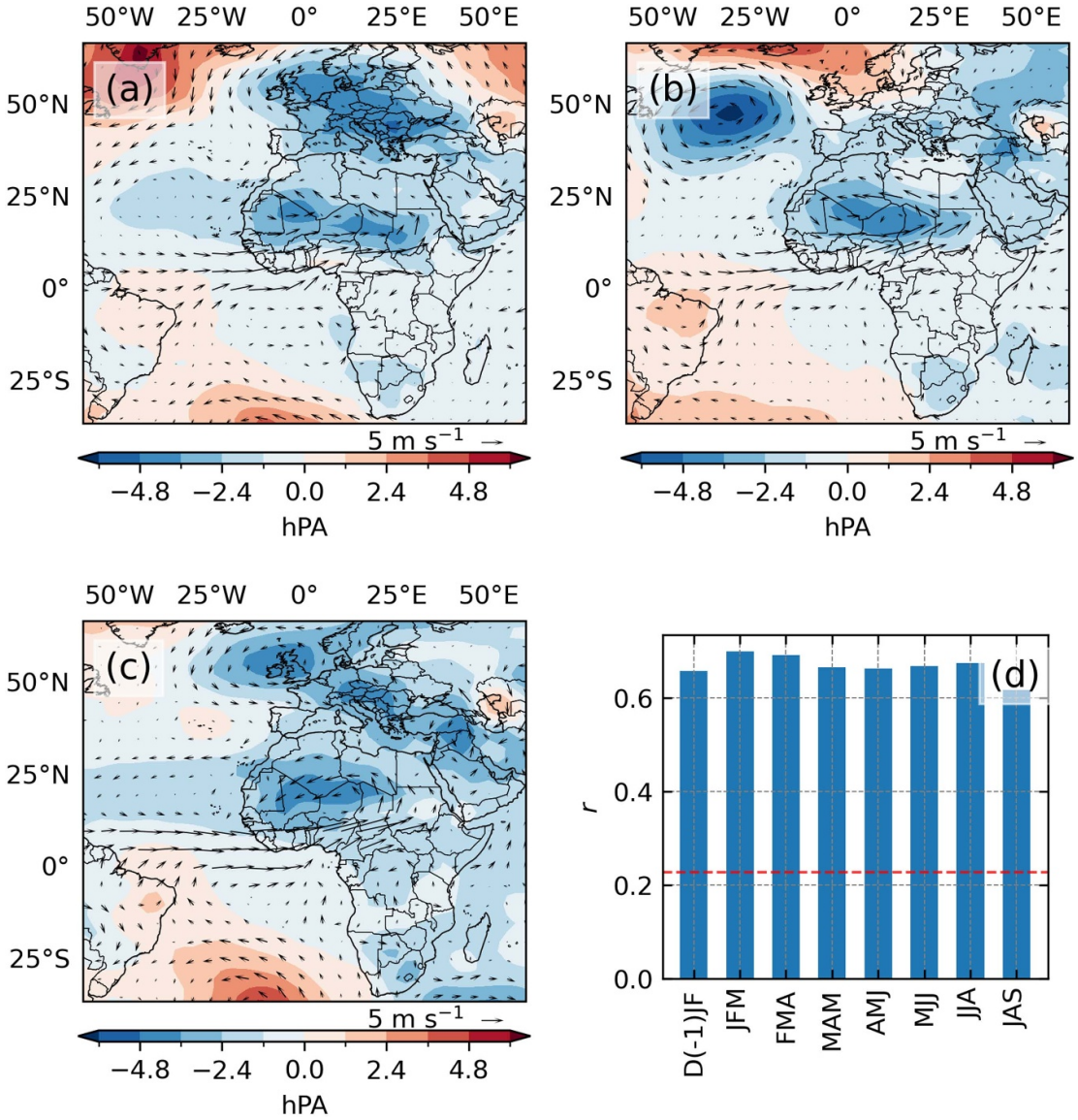

Figure 2. Regression of seasonal SLP (shading) and 850-hPa wind (vectors) anomalies onto SSTIDw for (a) D(−1)JF, (b) MAM, (c) JAS, and (d) lead-lag correlation SSTIDw and seasonal westerly indices from D(−1)JF to JAS. Red dashed line in (d) indicate significance at 5% level.

The SSTIDw is linked to negative anomalies of the Sahel (figure S2). Evolution of negative anomalies indicates increased cloud cover and deep convection over the Sahel during the positive SSTIDw phase. Prior to the establishment of the WAM in Sahel in summer (Sultan and Janicot 2003), the regions of lowest negative OLR anomalies are centered around the Guinea coast and Sudan (figures S2(a) and (b)).

Figure S3 shows the seasonal evolution of anomalies of the latitude-height cross section of vertical velocity and meridional wind vectors. During the positive SSTIDw phase in summer, the emergence of cells of vertical motion is observed, with a fully established deep vertical cell centered around 10° to 20° N in summer (figure S3(c)). However, the SHL results in a shallow cell centered around 20° N (Raj *et al* 2019). This coincides with the zonal band of maximum negative OLR anomalies centered around the central Sahel (figure S3(c)).

The mechanism for this delayed SSTIDw-SSR relationship is investigated. For this purpose, we examine the evolution of SSTID from the preceding winter to summer. There exists a statistically significant correlation coefficient between SSTIDw and the succeeding seasonal SSTID indices, which highlights the strong persistence of the SSTIDw anomalies from winter to summer (figure 3(a)). SST anomalies can both be a response to and drivers of atmospheric circulation. We study the response of moisture flux anomalies and convergence at the 850 hPa level and geopotential height anomalies at the 500 hPa level. Water vapor transport from the adjacent Atlantic Ocean plays a significant role in SSR variability. As the West African Westerly Jet (WWJ) intensifies in

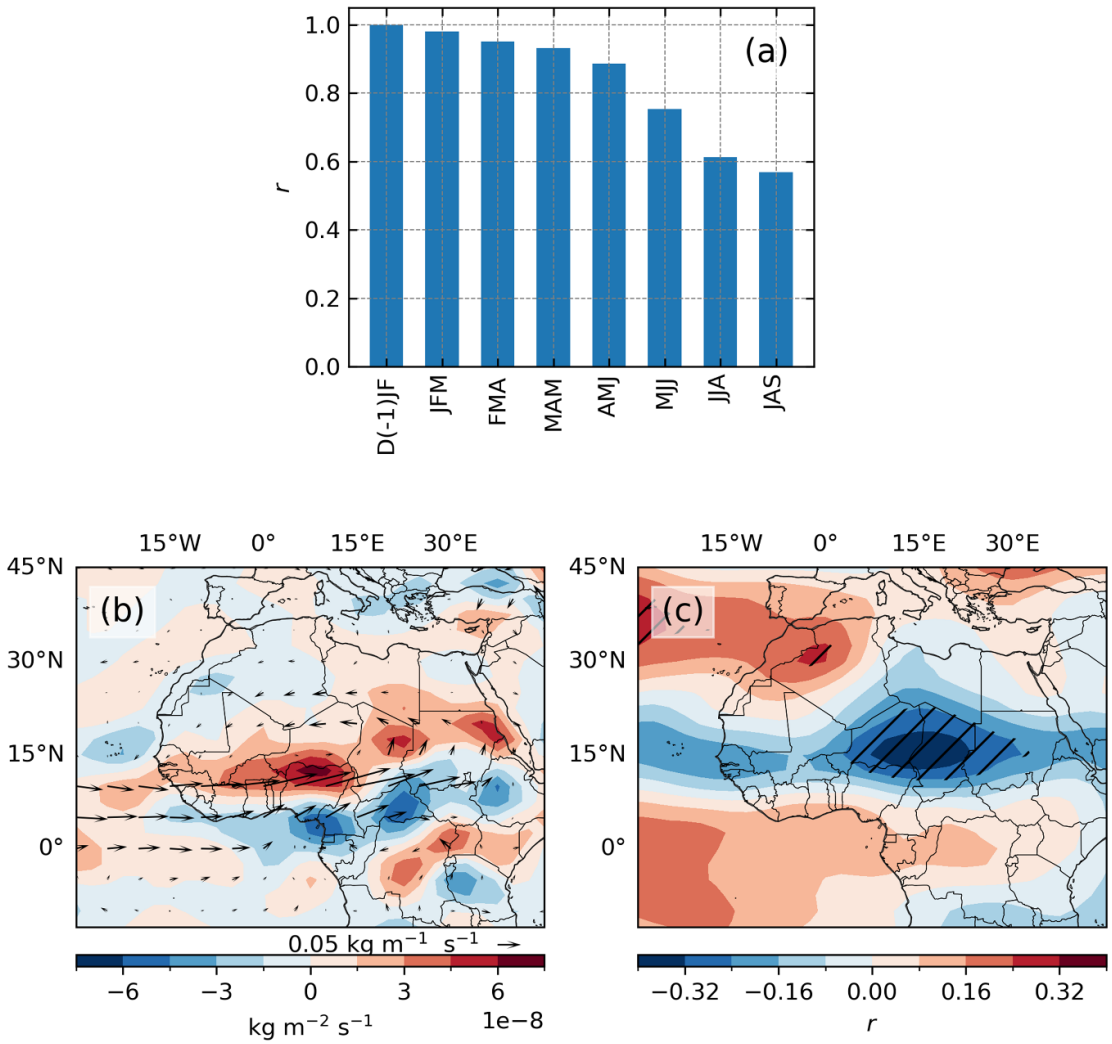

Figure 3. (a) Lead-lag correlation between SSTIDw and seasonal SSTID indices (D(−1)JF, JFM, FMA, …, JAS) during 1950–2023. (b) Regression of JAS 850 hPa moisture flux convergence (shading) and moisture flux (vectors) onto SSTIDw, (c) correlation map of SSTIDw with summer 500-hPa geopotential height over tropical northern Africa; shadings indicate significance at 5% level.

the peak of the monsoon season, moisture is transported northward, reaching 20° N, which is even more enhanced in relatively wet years (Lélé *et al* 2015). Anomalous 850 hPa moisture flux and convergence are shown as regression coefficients onto SSTIDw (figure 3(b)), while the correlation coefficient between 500 hPa geopotential and SSTIDw is shown in figure 3(c). Enhanced westerly moisture flux and positive anomalous convergence are induced by positive anomalous SSTIDw. These moisture anomalies are favorable for enhancing Sahel rainfall. Note that a meridional tripole of correlation coefficients is observed with a negative correlation centered around 15°N across the Sahel and positive correlation patterns to its north and south. This pattern coincides with enhanced vertical motion and negative OLR anomalies (figures S2 and S3), all of which are linked to moisture advection and deep convection in the Sahel (Nicholson 2009, Lélé *et al* 2015, Akinsanola and Zhou 2020).

3.3. Statistical model

In this section, we leverage this relationship to construct a linear regression predictive model. Here, we fit a linear regression model of the form:

$$\boldsymbol{SSR} = \beta_0 + \beta_1 \boldsymbol{SSTID_W} + \varepsilon.$$

Here β_0 is the intercept, β_1 is the regression coefficient, and ε is the residual, $\boldsymbol{SSR}$ and $\boldsymbol{SSTID_W}$ are the response and predictor variables, respectively. We have applied 70% of the data (1950–2001) as a training set and the remaining 30% (2002–2023) for independent evaluation. This approach is widely applied in predictive modeling (Li *et al* 2022), as robust model skill relies on an adequate balance between training and testing datasets, which reduces overfitting and ensures model generalizability (Xu and Goodacre 2018). The model realistically reproduced the key characteristics of SSR variability. Notably, the wet phase (1950s–1960s), the

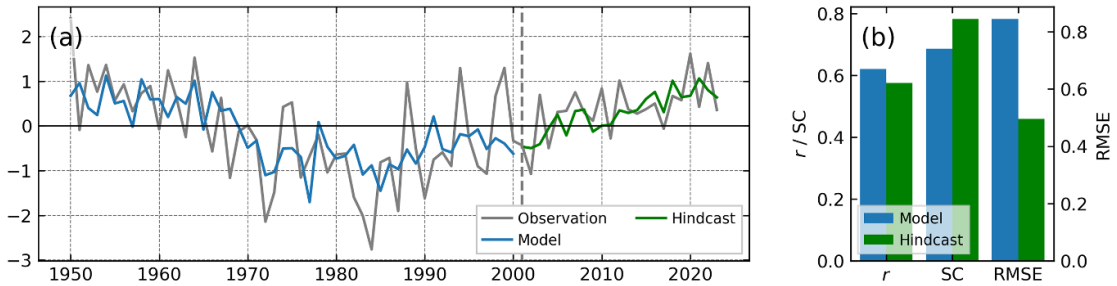

Figure 4. (a) Time series of the SSR index (gray line), model (blue line; 1950–2001), and independent hindcast results (green line; 2002–2023). (b) Evaluation metrics comparing model (blue bars) and hindcast (green bars) performance, including correlation coefficient (r), root mean square error (RMSE), and sign consistency (SC).

subsequent dry phase (1970s–1980s), and the 'partial recovery' period (post-1990s) have been reproduced, however, not without biases (figure 4(a)). Additionally, to evaluate the model's goodness of fit and predictive skill on the independent hindcast period, we employed correlation coefficient (r), sign consistency (SC), and RMSE. Although the model exhibits a stronger correlation (0.62) than the hindcast (0.58), the hindcast shows better performance in terms of SC and RMSE (78% and 0.5) compared to the model (69% and 0.84, figure 4(b)). Although marginal differences are seen in goodness of fit and predictive skill, suggesting confidence in practical applicability.

4. Discussion and conclusion

In the study, we analyzed the SSR and its relationship with SSTID (Sun *et al* 2013). Our analysis revealed statistically significant correlations between SSR and seasonal SSTID from preceding winter through summer, consistent with previous studies (Folland *et al* 1986, 1991). Moreover, we showed that this relationship is strongest between SSR and SSTIDw, suggesting predictive capability. We found this relationship to be robust and stationary compared to individual ocean basins. The interhemispheric dipole shapes Sahel rainfall by modulating the ITCZ (Folland *et al* 1986, Sun *et al* 2013). We maintain that the SSTID persists from winter to summer, acting on circulation features in West Africa, favoring increased monsoon flow and enhanced moisture convergence over the Sahel.

Furthermore, we demonstrate a skillful model for SSR rainfall prediction based on global-scale SST signals from the preceding winter. Notably, previous studies have highlighted the skill of global or regional spring SST anomalies in predicting SSR (Badr *et al* 2014, Folland *et al* 1991, Hulme *et al* 1992). Although direct comparison of results requires careful considerations due to cross-study inconsistencies, such as non-uniform data sampling, definition of the global-scale SST mode, and the empirical model used, among others. For instance, (Folland *et al* 1986, 1991) used annual rainfall anomalies in the Sahel from 1901–1987, while (Badr *et al* 2014) indicated the superiority of using the ANN. Nevertheless, we not only demonstrate the stationarity of the global-scale SST mode and SSR relationship but also reveal the importance of this association during the preceding winter.

In one of the world's most climate-vulnerable regions, the usefulness of predictions for decision-making in climate risk management heavily relies on their accuracy and lead time. Our findings demonstrate the potential to extend this lead time at no cost to predictive skill, enhancing early warning capability. However, under anthropogenic warming, persistent ocean conditions are projected to decline, with the most pronounced decline on the sea surface (Shi *et al* 2022). This may present challenges for the persistence-based empirical models, such as the one presented here. Furthermore, the results presented here provide a foundation for future dynamical modeling studies, which are necessary to test and confirm the physical mechanisms discussed.

Data availability statement

The data that support the findings of this study are openly available at the following URL/DOI: The Climate Research Unit Time Series (CRU TS) from the University of East Anglia's Climatic Research Unit (CRU) (https://crudata.uea.ac.uk/cru/data/hrg/). Extended Reconstructed Sea Surface Temperature (ERSST) (https://doi.org/10.7289/V5T72FNM). The NCEP-NCAR Reanalysis 1 (https://psl.noaa.gov/data/reanalysis/reanalysis.shtml).

Acknowledgment

This work was jointly supported by the National Natural Science Foundation of China (42288101), Laoshan Laboratory (No. LSKJ202202600), Shandong Natural Science Foundation Project (ZR2019ZD12), and Fundamental Research Funds for the Central Universities (202242001).

ORCID iD

Jianping Li 0000-0003-0625-1575

References

Akinsanola A A and Zhou W 2020 Understanding the variability of West African summer monsoon rainfall: contrasting tropospheric features and monsoon index *Atmosphere* **11** 309

An Q, Li J and Yang J 2024 Evaluation of sea surface temperature interhemispheric dipole in CMIP6 historical simulations *Clim. Dyn.* **62** 10347–62

Badr H S, Zaitchik B F and Guikema S D 2014 Application of statistical models to the prediction of seasonal rainfall anomalies over the sahel *J. Appl. Meteorol. Climatol.* **53** 614–36

Biasutti M 2013 Forced Sahel rainfall trends in the CMIP5 archive *J. Geophys. Res. Atmos.* **118** 1613–23

Biasutti M 2019 Rainfall trends in the African Sahel: characteristics, processes, and causes *WIREs Clim. Change* **10** e591

Diakhaté M, Rodríguez-Fonseca B, Gómara I, Mohino E, Dieng A L and Gaye A T 2019 Oceanic forcing on interannual variability of sahel heavy and moderate daily rainfall *J. Hydrometeorol.* **20** 397–410

Folland C, Owen J, Ward M N and Colman A 1991 Prediction of seasonal rainfall in the sahel region using empirical and dynamical methods *J. Forecasting* **10** 21–56

Folland C, Palmer T N and Parker D E 1986 Sahel rainfall and worldwide sea temperatures, 1901–85 *Nature* **320** 602–7

Giannini A, Ali A, Kelley C P, Lamptey B L, Minoungou B and Ndiaye O 2020 Advances in the lead time of sahel rainfall prediction with the North American multimodel ensemble *Geophys. Res. Lett.* **47** e2020GL087341

Giannini A, Saravanan R and Chang P 2003 Oceanic forcing of sahel rainfall on interannual to interdecadal time scales *Science* **302** 1027–30

Haarsma R J, Selten F M, Weber S L and Kliphuis M 2005 Sahel rainfall variability and response to greenhouse warming *Geophys. Res. Lett.* **32** L17702

Harris I, Osborn T J, Jones P and Lister D 2020 Version 4 of the CRU TS monthly high-resolution gridded multivariate climate dataset *Sci. Data* **7** 109

He Y, Wang B, Liu J, Wang Y, Li L, Liu L, Xu S, Huang W and Lu H 2024 Assessment of the decadal prediction skill of sahel rainfall in CMIP5 and CMIP6 *J. Clim.* **37** 2471–90

Huang B, Thorne P W, Banzon V F, Boyer T, Chepurin G, Lawrimore J H, Menne M J, Smith T M, Vose R S and Zhang H-M 2017 Extended reconstructed sea surface temperature, version 5 (ERSSTv5): upgrades, validations, and intercomparisons *J. Clim.* **30** 8179–205

Hulme M, Biot Y, Borton J, Buchanan-Smith M, Davies S, Folland C, Nicholds N, Seddon D and Ward N 1992 Seasonal rainfall forecasting for Africa part II—application and impact assessment *Int. J. Environ. Stud.* **40** 103–21

Islam M, Hasan M, Mia M, Md S, Al Masud A and Islam A R M T 2025 Early warning systems in climate risk management: roles and implementations in eradicating barriers and overcoming challenges *Nat. Hazards Res.* (https://doi.org/10.1016/j.nhres.2025.01.007)

Janicot S, Trzaska S and Poccard I 2001 Summer Sahel-ENSO teleconnection and decadal time scale SST variations *Clim. Dyn.* **18** 303–20

Kalnay E *et al* 1996 The NCEP/NCAR 40-Year reanalysis project *Bull. Am. Meteorol. Soc.* **77** 437–72

Lélé M I, Leslie L M and Lamb P J 2015 Analysis of low-level atmospheric moisture transport associated with the West African monsoon *J. Clim.* **28** 4414–30

Li J, Xie T, Tang X, Wang H, Sun C, Feng J, Zheng F and Ding R 2022 Influence of the NAO on wintertime surface air temperature over east asia: multidecadal variability and decadal prediction *Adv. Atmos. Sci.* **39** 625–42

Losada T, Rodriguez-Fonseca B, Mohino E, Bader J, Janicot S and Mechoso C R 2012 Tropical SST and sahel rainfall: a non-stationary relationship *Geophys. Res. Lett.* **39** L12705

Martín-Gómez V, Mohino E, Rodríguez-Fonseca B and Sánchez-Gómez E 2022 Understanding rainfall prediction skill over the Sahel in NMME seasonal forecast *Clim. Dyn.* **59** 3113–33

Mo K C and Thiaw W M 2002 Ensemble canonical correlation prediction of precipitation over the Sahel *Geophys. Res. Lett.* **29** 11–1–11–4

Mohino E, Janicot S and Bader J 2011 Sahel rainfall and decadal to multi-decadal sea surface temperature variability *Clim. Dyn.* **37** 419–40

Nicholson S E 2009 A revised picture of the structure of the "monsoon" and land ITCZ over West Africa *Clim. Dyn.* **32** 1155–71

Nicholson S E 2018 Climate of the sahel and West Africa *Oxford Research Encyclopedia of Climate Science* (Oxford University Press) (https://doi.org/10.1093/acrefore/9780190228620.013.510)

Nicholson S E, Fink A H and Funk C 2018 Assessing recovery and change in West Africa's rainfall regime from a 161-year record *Int. J. Climatol.* **38** 3770–86

Nicholson S E and Webster P J 2007 A physical basis for the interannual variability of rainfall in the Sahel *Q. J. R. Meteorol. Soc.* **133** 2065–84

Parker D J, Thorncroft C D, Burton R R and Diongue-Niang A 2005 Analysis of the African easterly jet, using aircraft observations from the JET2000 experiment *Q. J. R. Meteorol. Soc.* **131** 1461–82

Pomposi C, Giannini A, Kushnir Y and Lee D E 2016 Understanding Pacific Ocean influence on interannual precipitation variability in the Sahel *Geophys. Res. Lett.* **43** 9234–42

Raj J, Bangalath H K and Stenchikov G 2019 West African Monsoon: current state and future projections in a high-resolution AGCM *Clim. Dyn.* **52** 6441–61

Sheen K L, Smith D M, Dunstone N J, Eade R, Rowell D P and Vellinga M 2017 Skilful prediction of Sahel summer rainfall on inter-annual and multi-year timescales *Nat. Commun.* **8** 14966

Shekhar R and Boos W R 2017 Weakening and shifting of the Saharan shallow meridional circulation during wet years of the West African monsoon *J. Clim.* **30** 7399–422

Shi H, Jin F-F, Wills R C J, Jacox M G, Amaya D J, Black B A, Rykaczewski R R, Bograd S J, García-Reyes M and Sydeman W J 2022 Global decline in ocean memory over the 21st century *Sci. Adv.* **8** eabm3468

Suárez Moreno R 2019 Modulation of the non-stationary mediterranean-sahel teleconnection *Interdecadal Changes in Ocean Teleconnections with the Sahel: Implications in Rainfall Predictability* ed R S Moreno (Springer) pp 155–74

Sultan B, Janicot S and Diedhiou A 2003 The West African monsoon dynamics. Part I: documentation of intraseasonal variability *J. Clim* **16** 3389–406

Sun C, Li J, Jin F-F and Ding R 2013 Sea surface temperature inter-hemispheric dipole and its relation to tropical precipitation *Environ. Res. Lett.* **8** 044006

Thorncroft C D, Nguyen H, Zhang C and Peyrillé P 2011 Annual cycle of the West African monsoon: regional circulations and associated water vapour transport *Q. J. R. Meteorol. Soc.* **137** 129–47

Xu Y and Goodacre R 2018 On splitting training and validation set: a comparative study of cross-validation, bootstrap and systematic sampling for estimating the generalization performance of supervised learning *J. Anal. Test.* **2** 249–62

Xue J, Wang B, Yu Y, Li J, Sun C and Mao J 2022 Multidecadal variation of northern hemisphere summer monsoon forced by the SST inter-hemispheric dipole *Environ. Res. Lett.* **17** 044033

Yaqian H and Lee E 2016 Empirical relationships of sea surface temperature and vegetation activity with summer rainfall variability over the sahel *Earth Interact* **20** 1–18